ELECTRONIC RESEARCH ARCHIVE doi:10.3934/era.2021032

A CONFORMING-NONCONFORMING MIXED IMMERSED FINITE ELEMENT METHOD FOR UNSTEADY STOKES EQUATIONS WITH MOVING INTERFACES

Derrick Jones

Department of Mathematics and Statistics, Mississippi State University
Mississippi State, MS 39762, USA

Xu Zhang*

Department of Mathematics, Oklahoma State University
Stillwater, OK 74078, USA

Abstract. In this article, we develop a new mixed immersed finite element discretization for two-dimensional unsteady Stokes interface problems with unfitted meshes. The proposed IFE spaces use conforming linear elements for one velocity component and non-conforming linear elements for the other velocity component. The pressure is approximated by piecewise constant. Unisolvency, among other fundamental properties of the new vector-valued IFE functions, is analyzed. Based on the new IFE spaces, semi-discrete and full-discrete schemes are developed for solving the unsteady Stokes equations with a stationary or a moving interface. Re-meshing is not required in our numerical scheme for solving the moving-interface problem. Numerical experiments are carried out to demonstrate the performance of this new IFE method.

1. **Introduction.** Let $\Omega \subset \mathbb{R}^2$ be an open bounded domain separated by a time-dependent smooth interface $\Gamma(t)$. The evolving interface $\Gamma(t)$ divides the domain Ω into two open subdomains $\Omega^+(t)$ and $\Omega^-(t)$ such that $\Omega = \Omega^+(t) \cup \Omega^-(t) \cup \Gamma(t)$, see Figure 1. Consider the following initial-boundary-value problems of the Stokes equation

$$\frac{\partial \mathbf{u}}{\partial t} - \nabla \cdot (\mu \nabla \mathbf{u} - p\mathbb{I}) = \mathbf{f} \quad \text{in } \Omega \times [0,T], \tag{1}$$

$$\nabla \cdot \mathbf{u} = 0 \quad \text{in } \Omega \times [0,T], \tag{2}$$

$$\mathbf{u} = \mathbf{0} \quad \text{on } \partial\Omega \times [0,T], \tag{3}$$

$$\mathbf{u}(\mathbf{x},0) = \mathbf{u}_0, \ p(\mathbf{x},0) = p_0 \quad \text{on } \Omega, \tag{4}$$

where $\mathbf{u}$ and p denote the flow velocity and the pressure, respectively. Functions $\mathbf{f}$, $\mathbf{u}_0$, and p_0 are the given body force, the initial velocity, and the initial pressure, respectively. $\mathbb{I}$ denotes the identity tensor. The movement of the interface is assumed

2020 *Mathematics Subject Classification.* Primary: 65N15, 65N30; Secondary: 35R05.

Key words and phrases. Conforming-nonconforming immersed finite element, Stokes interface problem, moving interface.

The first author is supported by NSF Graduate Research Fellowship NO. 1645630. The second author is supported by NSF Grants DMS-1720425 and DMS-2005272.

* Corresponding author.

to be guided by a given velocity field $\mathbf{v}(\mathbf{x},t)$ as follows

$$\frac{d\mathbf{x}}{dt} = \mathbf{v}(\mathbf{x},t), \text{ on } \Gamma(t)\times[0,T]. \tag{5}$$

The viscosity function $\mu(\mathbf{x})$ is assumed to have a finite jump across the interface $\Gamma(t)$. For simplicity, we assume that $\mu(\mathbf{x})$ is a piecewise constant function

$$\mu(\mathbf{x}) = \begin{cases} \mu^- & \text{in } \Omega^-(t), \\ \mu^+ & \text{in } \Omega^+(t), \end{cases} \tag{6}$$

where $\mu^\pm > 0$ and $\mathbf{x} = (x,y)$. At any time t, the velocity and the stress tensors satisfy the following homogeneous interface jump conditions

$$[\![\mathbf{u}]\!]_\Gamma = 0, \tag{7}$$

$$[\![(\mu\nabla\mathbf{u} - p\mathbb{I})\mathbf{n}]\!]_\Gamma = \mathbf{0}, \tag{8}$$

where the jump $[\![\mathbf{v}(\mathbf{x})]\!]_\Gamma := \mathbf{v}^+(\mathbf{x})|_\Gamma - \mathbf{v}^-(\mathbf{x})|_\Gamma$, and $\mathbf{n}$ denotes the unit normal vector to the interface Γ pointing from $\Omega^-(t)$ to $\Omega^+(t)$.

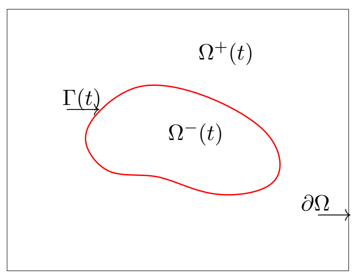

Figure 1: A sketch of the domain for the moving interface problem.

FIGURE 1. The geometrical setup of a moving interface problem.

Numerical approximations of the Stokes equation have been extensively studied for many years due to its wide applicability to model natural phenomena such as airflow, water flow, and ocean currents. The family of Taylor-Hood finite elements [35] uses conforming P_k-P_{k-1} pairs to approximate the velocity and pressure requiring the polynomial degree $k \geq 2$. To use low-order polynomials and preserve the mass conservation property, nonconforming finite element methods [4] and discontinuous Galerkin methods [33] have been widely used. Crouzeix and Raviart introduced the lowest-order nonconforming P_1-P_0 finite element [6], which is well-known as the CR finite element. On quadrilateral meshes, Rannacher and Turek developed a nonconforming rotated-Q_1 element in [32]. These nonconforming finite elements make use of low-order polynomials and they are elementwise divergence-free [2, 23]. A mixed conforming-nonconforming finite element space was introduced in [21]. In this discretization, one velocity component is approximated by the conforming P_1 element and the other one is approximated by the nonconforming P_1 element, while the pressure is piecewise constant. This mixed FEM construction has advantages over the CR element in handling the Neumann boundary condition [21], and it is computationally less expensive than the CR element. This mixed conforming-nonconforming FEM has also been extended to the 3D Stokes equation [38]. For more details regarding numerical methods for Stokes equations, we refer readers to [8, 19].

Traditional numerical methods use interface-fitted meshes for solving interface problems. For fluid flow interface problems, the arbitrary Lagrangian-Eulerian

If the interface does not change with respect to time, then conventional finite element methods [36] can solve parabolic interface problems satisfactorily provided that body-fitting meshes are used [2, 4, 6]. A body-fitting mesh has to be constructed according to the interface such that each element is essentially on one side of the interface and only touches the interface on its vertices, see the illustration in Figure 2. Otherwise sub-optimal convergence will occur [3]. This restriction can cause the difficulties when applying traditional finite elements to solve moving interface problems, some of them are:

- Whenever the interface changes in the computation, a new mesh has to be generated according to the new location of the moving interface in order to satisfy the body-fitting restriction, which is a time-consuming task in many applications.
- Finite element spaces based body-fitting meshes generated at two time levels often have different degree of freedoms unless extra procedures are employed to keep them the same. If the trial and test spaces in a bilinear form of a finite element method are on different time levels, they will have different dimensions; hence, the related matrix in the algebraic system of this finite element method cannot be square, which demands for extra efforts to solve the algebraic system.
- One main feature of finite element computation is the so called "local assembling" idea, by which a matrix in the algebraic system of a finite element method is generated by computing the related quantities locally on each element of a mesh and then assembling these local quantities globally into the matrix. However, when assembling the matrix defined by a bilinear form whose trial and test spaces are on different meshes due to the body-fitting restriction for a moving interface, an element of one mesh may or may not be that of another mesh, which essentially makes the "local assembling" idea not applicable. This lack of "local" feature will lead to more complicated programming and can increase computational cost even further by a significant amount.
- Moreover, some of the traditional numerical techniques may become inefficient or even obsolete when body-fitting meshes are used for moving interface problems. Recall that semi-discretization methods solve an initial-boundary value problem of a parabolic equation by forming an ordinary differential equation (ODE) system through the discretization in the spatial variable. However, such an ODE system is not well defined when body-fitting mesh has to be used because of the indefiniteness of the dimension of the finite element space and the indefiniteness of the locations of global degree of freedoms. In particular, this limitation makes popular methods such as the method of lines [33, 35, 42], which semi-discretizes the original PDE into a system of ODEs and then solves them by any desired ODE solver, inapplicable due to the lack of "lines".

On the other hand, the advantage of a Cartesian mesh is clearer when the simulations or physical models require structured meshes for interface problems, such as Particle-In-Cell method for plasma particle simulations [28, 29, 38, 39]. It is therefore desirable to develop numerical methods for moving interface problems that can be carried out on a mesh independent of the interface and allow the interface to cut

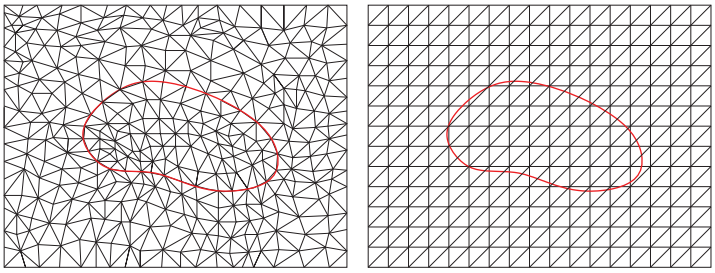

FIGURE 2. From left: an interface-fitted mesh and an unfitted mesh.

(ALE)-based finite element is a popular numerical method [7, 22, 37]. Recently, there has been a growing interest in developing unfitted-mesh numerical methods for solving a variety of interface problems, see Figure 2. Comparing with conventional fitted-mesh methods, such as classical FE and DG methods, the unfitted-mesh methods do not require the alignment of the mesh with a prescribed nontrivial interface; hence it is more desirable for time-dependent problems with moving interfaces. In the past decades, several unfitted-mesh methods have been developed for solving Stokes interface problems, such as CutFEM [15], Nitsche's FEM [36], XFEM[9], fictitious domain FEM [31, 34], to name only a few. The immersed finite element method (IFEM) [24, 26, 18, 11, 14, 30] is a class of unfitted-mesh finite element methods for solving interface problems. The main idea of IFEM is to incorporate the interface jump conditions in the construction of IFE basis functions. Unlike other aforementioned unfitted-mesh methods, the IFE space is isomorphic to the standard FE space with no interface. Consequently, not only is the mesh independent of the interface in an IFEM, but also the number and the location of the degrees of freedom are interface-independent. For time-dependent interface problems with a moving interface, the linear system has the same size at each time level and the nonzero entries remain at the same locations [10, 12, 13, 16, 17]. Moreover, the method-of-lines technique can be utilized together with IFEM for solving moving interface problems [25].

There have been some IFE methods developed for steady-state Stokes interface problems. In [1, 3] the Q_1-Q_0 immersed DG method was introduced. The velocity is approximated by the broken Q_1 functions while the pressure is approximated by the piecewise constant functions. The computational framework is based on the interior penalty DG method [33]. Based on the nonconforming finite element framework [6, 32], a class of nonconforming IFE approximations was developed [20]. Recently, a P_2-P_1 Taylor-Hood IFE space was introduced in [5]. The partially penalized IFE scheme is used with ghost penalty for enhancing the stability of numerical scheme especially for the pressure approximation.

The goal of this paper is two-fold. First, we develop a lowest-order conforming-nonconforming mixed IFE space for the Stokes equation based on [21]. Comparing with the IDG method [1] and the Taylor-Hood IFE method [5], our new IFE method has no additional consistency and stability terms, so the numerical formulation is much simpler to implement. Comparing with the CR-P_0 IFE space [20], there are significantly less degrees of freedom due to the conformity of one velocity component. In fact, on the same triangular mesh, only two-thirds of degrees of freedom

are required for velocity in this new mixed IFEM. Besides, the mixed conforming-nonconforming finite element is robust for handling both Dirichlet and Neumann boundary conditions, while the CR finite element space is only stable for Dirichlet boundary conditions [21].

The second goal is to apply this mixed IFE method for solving unsteady Stokes equations with a moving interface. We will use the new vector-valued IFE spaces for semi-discretization, and use the prototypical backward-Euler and Crank-Nicolson scheme for full-discretization. Our method does not require re-meshing at any time level. Since the degrees of freedom are also independent of the interface, there is no need to overhaul the global matrices at each time level. Instead, only local modification is carried out on elements where the interface configuration changed during two consecutive time steps.

The rest of the paper is organized as follows. In Section 2, we construct the new mixed IFE spaces for Stokes equations. In Section 3, we report some fundamental properties of the new IFE spaces. In section 4, we present the semi-discrete and the full-discrete IFE method for solving unsteady Stokes interface problems with a moving interface. Some numerical examples are reported in Section 5. A brief conclusion is given in Section 6.

2. Mixed conforming-nonconforming immersed finite element spaces.

In this section, we introduce the mixed conforming-nonconforming IFE spaces for Stokes equations. Let $\mathcal{T}_h = \{T\}$ be an interface-unfitted triangulation of a polygonal domain Ω. Let $\mathcal{N}_h$ and $\mathcal{E}_h$ denote the collections of nodes and edges of the mesh $\mathcal{T}_h$, respectively. Elements in $\mathcal{T}_h$ are divided into two categories: an interface element if T is cut through by the interface Γ, and a non-interface element otherwise. The collections of interface elements and non-interface elements are denoted by $\mathcal{T}_h^i$ and $\mathcal{T}_h^n$, respectively. Similarly, for each edge $e \in \mathcal{E}_h$, if e intersects the interface, it is called an interface edge; otherwise it is a non-interface edge. The collections of interface edges and non-interface edges are denoted by $\mathcal{E}_h^i$ and $\mathcal{E}_h^n$, respectively. Additionally, we let $\mathring{\mathcal{E}}_h$ and $\mathcal{E}_h^b$ be the collections of internal edges and boundary edges, respectively. Let $\mathring{\mathcal{N}}_h$ and $\mathcal{N}_h^b$ be the collections of internal nodes and boundary nodes, respectively. We also assume that the triangulation $\mathcal{T}_h$ satisfies the following hypotheses [28]:

- **(H1)** The interface Γ cannot intersect an edge of any element at more than two points unless the edge is part of Γ.
- **(H2)** If Γ intersects the boundary of an element at two points, these intersection points must be on different edges of this element.
- **(H3)** The interface Γ is a piecewise C^2-continuous function, and the mesh $\mathcal{T}_h$ is formed such that the subset of Γ in every interface element is C^2-continuous.

2.1. Conforming-nonconforming FE spaces.

Let $T \in \mathcal{T}_h^n$ be a non-interface element with vertices A_1, A_2, A_3 oriented counterclockwise. We label the edges of T by $e_1 = \overline{A_1A_2}$, $e_2 = \overline{A_2A_3}$, and $e_3 = \overline{A_3A_1}$. Let $\lambda_{j,T} \in \mathcal{P}_1$ be the Lagrange linear nodal basis functions such that

$$\lambda_{j,T}(A_i) = \delta_{ij}, \ i,j = 1,2,3, \tag{9}$$

where δ_{ij} is the Kronecker function. Define $\psi_{j,T} = 1 - 2\lambda_{k_j,T}$ with $k_1 = 3$, $k_2 = 1$, and $k_3 = 2$. It can be verified that $\psi_{j,T}$ satisfies the mean-value conditions, namely,

$$\frac{1}{|e_i|}\int_{e_i} \psi_{j,T}(x,y)ds = \delta_{ij},\ i,j = 1,2,3. \tag{10}$$

Thus $\psi_{j,T}$, $j = 1,2,3$ are nonconforming-$\mathcal{P}_1$ (CR) basis functions on T. The pressure is approximated by the piecewise constant function space denoted by $\mathcal{P}_0$. On each non-interface triangle $T \in \mathcal{T}_h^n$, the vector-valued CR-P_1-P_0 finite element space can be written as $\mathbf{S}_h^n(T) = \mathcal{P}_1 \times \mathcal{P}_1 \times \mathcal{P}_0$, or quivalently, $\mathbf{S}_h^n(T) = \text{span}\{\boldsymbol{\psi}_{i,T} : 1 \le i \le 7\}$ where the vector-valued basis functions are given below

$$\boldsymbol{\psi}_{j,T} = \begin{pmatrix} \psi_{j,T} \\ 0 \\ 0 \end{pmatrix},\ j = 1,2,3,\ \boldsymbol{\psi}_{j,T} = \begin{pmatrix} 0 \\ \lambda_{j-3,T} \\ 0 \end{pmatrix},\ j = 4,5,6,\ \boldsymbol{\psi}_{7,T} = \begin{pmatrix} 0 \\ 0 \\ 1 \end{pmatrix}. \tag{11}$$

Similarly, we can also form the P_1-CR-P_0 finite element space using conforming-$\mathcal{P}_1$ bases for the first component, and the nonconforming-$\mathcal{P}_1$ in the second component, then the basis functions are

$$\tilde{\boldsymbol{\psi}}_{j,T} = \begin{pmatrix} \lambda_{j,T} \\ 0 \\ 0 \end{pmatrix},\ j = 1,2,3,\ \tilde{\boldsymbol{\psi}}_{j,T} = \begin{pmatrix} 0 \\ \psi_{j-3,T} \\ 0 \end{pmatrix},\ j = 4,5,6,\ \tilde{\boldsymbol{\psi}}_{7,T} = \begin{pmatrix} 0 \\ 0 \\ 1 \end{pmatrix}. \tag{12}$$

The P_1-CR-P_0 finite element space is $\tilde{\mathbf{S}}_h^n(T) = \text{span}\{\tilde{\boldsymbol{\psi}}_{i,T} : 1 \le i \le 7\}$. Note that these two spaces $\mathbf{S}_h^n(T)$ and $\tilde{\mathbf{S}}_h^n(T)$ are identical, both equal $\mathcal{P}_1 \times \mathcal{P}_1 \times \mathcal{P}_0$. However, the degrees of freedom of $\mathbf{S}_h^n(T)$ and $\tilde{\mathbf{S}}_h^n(T)$ are different, as indicated in (9) and (10). For more details of the conforming-nonconforming finite elements, we refer readers to [21].

2.2. **Mixed conforming-nonconforming IFE spaces.** In this subsection, we extend these conforming-nonconforming finite elements to the IFE spaces on each interface triangle $T \in \mathcal{T}_h^i$. Let $A_i = (x_i, y_i)$, $i = 1,2,3$ be the vertices of T. Without loss of generality, we consider the reference triangle whose vertices are given by

$$\hat{A}_1 = (0,0),\ \hat{A}_2 = (1,0),\ \hat{A}_3 = (0,1).$$

Note that an arbitrary triangle with vertices $A_i = (x_i, y_i)$, $i = 1,2,3$ can be mapped to this reference triangle by the following mapping

$$\begin{pmatrix} \hat{x} \\ \hat{y} \end{pmatrix} = \begin{pmatrix} x_2 - x_1 & x_3 - x_1 \\ y_2 - y_1 & y_3 - y_1 \end{pmatrix}^{-1} \begin{pmatrix} x - x_1 \\ y - y_1 \end{pmatrix}. \tag{13}$$

To simplify the notation, we still use x, y, rather than $\hat{x}$, $\hat{y}$ on the reference triangle. According to the hypotheses (H1)-(H3), there are two distinct intersection points on each interface triangle, denoted by $D = (x_d, y_d)$ and $E = (x_e, y_e)$, on two different edges. There are generally three types of interface triangles as depicted in Figure 3. The line segment $\overline{DE}$ is used to approximate the actual interface curve $\Gamma \cap T$, and it divides the element T into two subelements, denoted by T^+ and T^-. For example, on a Type I interface element, $D = A_1 + d(A_2 - A_1)$ and $E = A_1 + e(A_3 - A_1)$ where $0 < d, e < 1$.

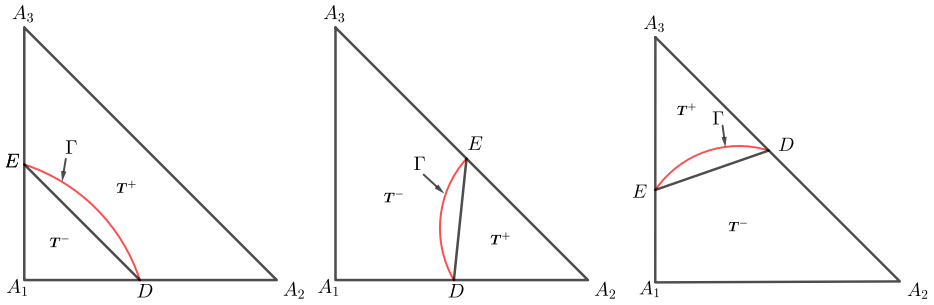

FIGURE 3. Types of interface elements. From left: Type I, Type II, Type III.

We construct the vector-valued IFE shape functions in terms of the FE functions $\boldsymbol{\psi}_{i,T}$ in (11). To be more precise, we have

$$\boldsymbol{\phi}_{j,T}(x,y) = \begin{cases} \sum_{i=1}^{7} c_{ij}^{+} \boldsymbol{\psi}_{i,T}(x,y), & \text{if } (x,y) \in T^+, \\ \sum_{i=1}^{7} c_{ij}^{-} \boldsymbol{\psi}_{i,T}(x,y), & \text{if } (x,y) \in T^-, \end{cases} \qquad j = 1, 2, \cdots, 7. \tag{14}$$

It can be observed that each vector-valued IFE shape function $\boldsymbol{\phi}_{j,T}$ has 14 unknown coefficients c_{ij}^{s}, with $1 \le i \le 7$ and $s = +, -$. These coefficients are determined by seven local degrees of freedom (prescribed nodal values, edge values, and the mean pressure value), six interface jump conditions, and a divergence free condition stated below.

- Three edge-value conditions:

$$\frac{1}{|e_k|} \int_{e_k} \boldsymbol{\phi}_{j,T} ds = \begin{pmatrix} \delta_{jk} \\ 0 \\ 0 \end{pmatrix}, \quad k = 1, 2, 3. \tag{15}$$

- Three nodal-value conditions:

$$\boldsymbol{\phi}_{j,T}(A_{k-3}) = \begin{pmatrix} 0 \\ \delta_{jk} \\ 0 \end{pmatrix}, \quad k = 4, 5, 6. \tag{16}$$

- One mean-pressure-value condition:

$$\frac{1}{|T|} \int_{T} \boldsymbol{\phi}_{j,T} dx dy = \begin{pmatrix} 0 \\ 0 \\ \delta_{jk} \end{pmatrix}, \quad k = 7. \tag{17}$$

- Four continuity conditions of the velocity to incorporate (7):

$$[\![\phi_{1,j}(D)]\!] = [\![\phi_{2,j}(D)]\!] = [\![\phi_{1,j}(E)]\!] = [\![\phi_{2,j}(E)]\!] = 0. \tag{18}$$

- Two stress continuity conditions to incorporate (8):

$$[\![\mu \left(\partial_x \phi_{1,j} n_1 + \partial_y \phi_{1,j} n_2\right) - \phi_{p,j} n_1]\!]_{\overline{DE}} = 0, \tag{19}$$

$$[\![\mu \left(\partial_x \phi_{2,j} n_1 + \partial_y \phi_{2,j} n_2\right) - \phi_{p,j} n_2]\!]_{\overline{DE}} = 0. \tag{20}$$

- One continuity of the divergence condition to incorporate (2):

$$[\![\partial_x \phi_{1,j} + \partial_y \phi_{2,j}]\!]_{\overline{DE}} = 0. \tag{21}$$

Here, in (18)-(21), the scalar function $\phi_{i,j}$ denotes the i-th component of $\boldsymbol{\phi}_{j,T}$. More precisely, we have $\boldsymbol{\phi}_{j,T} = (\phi_{1,j}, \phi_{2,j}, \phi_{p,j})$ such that $\boldsymbol{\phi}_{j,T}|_{T^s} = \boldsymbol{\phi}^s_{j,T} = (\phi^s_{1,j}, \phi^s_{2,j}, \phi^s_{p,j}) \in \mathcal{P}_1 \times \mathcal{P}_1 \times \mathcal{P}_0$, with $s = +, -$. Combining the conditions (15)-(21) yields a linear system of fourteen unknowns. On Type I interface element, we have

$$M_{\mathrm{I}} \mathbf{c}_j = \mathbf{e}_j \tag{22}$$

where the coefficient matrix M_{I} is written as the first seven columns and the next seven seven columns due to width limit of the page:

$$M_{\mathrm{I}}(:, 1:7) = \begin{pmatrix} d & d^2-d & d-d^2 & 0 & 0 & 0 & 0 \\ 0 & 0 & 0 & 0 & 0 & 0 & 0 \\ e-e^2 & e^2-e & e & 0 & 0 & 0 & 0 \\ 0 & 0 & 0 & 1 & 0 & 0 & 0 \\ 0 & 0 & 0 & 0 & 0 & 0 & 0 \\ 0 & 0 & 0 & 0 & 0 & 0 & 0 \\ 0 & 0 & 0 & 0 & 0 & 0 & de \\ -1 & 1-2d & 2d-1 & 0 & 0 & 0 & 0 \\ 0 & 0 & 0 & d-1 & -d & 0 & 0 \\ 2e-1 & 1-2e & -1 & 0 & 0 & 0 & 0 \\ 0 & 0 & 0 & e-1 & 0 & -e & 0 \\ -2d & 2d+4e & -4e & -d & d & 0 & -e \\ -2e & 2e & 0 & -2d-e & e & 2d & -d \\ 0 & -2 & 2 & 1 & 0 & -1 & 0 \end{pmatrix}$$

and

$$M_{\mathrm{I}}(:, 8:14) = \begin{pmatrix} 1-d & d-d^2 & d^2-d & 0 & 0 & 0 & 0 \\ 0 & 1 & 0 & 0 & 0 & 0 & 0 \\ e^2-e & e-e^2 & 1-e & 0 & 0 & 0 & 0 \\ 0 & 0 & 0 & 0 & 0 & 0 & 0 \\ 0 & 0 & 0 & 0 & 1 & 0 & 0 \\ 0 & 0 & 0 & 0 & 0 & 1 & 0 \\ 0 & 0 & 0 & 0 & 0 & 0 & 1-de \\ 1 & 2d-1 & 1-2d & 0 & 0 & 0 & 0 \\ 0 & 0 & 0 & 1-d & d & 0 & 0 \\ 1-2e & 2e-1 & 1 & 0 & 0 & 0 & 0 \\ 0 & 0 & 1-e & 0 & e & 0 & \\ 2d\rho & -2(d+2e)\rho & 4e\rho & d\rho & -d\rho & 0 & e \\ 2e\rho & -2e\rho & 0 & (2d+e)\rho & -e\rho & -2d\rho & d \\ 0 & 2 & -2 & -1 & 0 & 1 & 0 \end{pmatrix}$$

with $\rho = \mu^+/\mu^-$ being the jump ratio. The unknown vector $\mathbf{c}_j$ and the right-hand-side vector $\mathbf{e}_j$ take the form

$$\begin{aligned} \mathbf{c}_j &= \left(c^+_{1j}, c^+_{2j}, c^+_{3j}, c^+_{4j}, c^+_{5j}, c^+_{6j}, c^+_{7j}, c^-_{1j}, c^-_{2j}, c^-_{3j}, c^-_{4j}, c^-_{5j}, c^-_{6j}, c^-_{7j}\right)^t, \\ \mathbf{e}_j &= \left(\delta_{j1}, \delta_{j2}, \delta_{j3}, \delta_{j4}, \delta_{j5}, \delta_{j6}, \delta_{j7}, 0, 0, 0, 0, 0, 0, 0\right)^t. \end{aligned}$$

We can obtain the vector-valued IFE shape functions $\boldsymbol{\phi}_{j,T}$ by solving for $\mathbf{c}_j$ with each vector $\mathbf{e}_j$, $j = 1, 2, \cdots, 7$. Note that the matrices for Type II and Type III

interface elements, denoted by M_{II} and M_{III}, can be derived in a similar fashion; hence, we omit the details in this paper.

As an illustration, we plot the three components of the CR-P_1-P_0 IFE shape function $\boldsymbol{\phi}_{4,T}$ in Figure 4. As a comparison, we plot the standard CR-P_1-P_0 FE shape function $\boldsymbol{\psi}_{4,T}$. We note that both FE and IFE shape functions are such that their second velocity components have the value one at the node A_1. However, due to the coupled stress jump condition (8), the first velocity component and the pressure component of the IFE shape function $\boldsymbol{\phi}_{4,T}$ are not completely zero, as the FE shape function. This is a similar phenomenon that also occurs in other vector-valued IFE functions [1, 20, 27, 29].

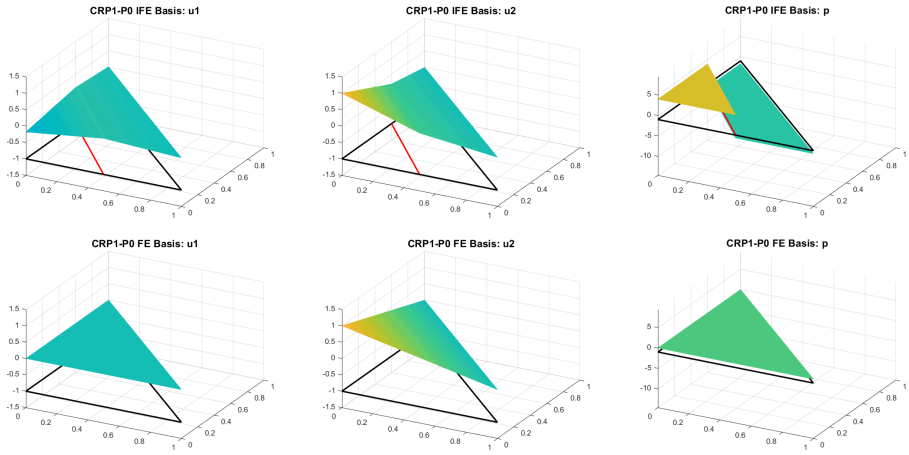

FIGURE 4. A comparison of the vector-valued IFE shape function $\boldsymbol{\phi}_{4,T}$ with $\mu^- = 1$, $\mu^+ = 5$ (top), and the corresponding FE shape function $\boldsymbol{\psi}_{4,T}$ (bottom) on the reference triangle.

The local CR-P_1-P_0 IFE space is formed by $\mathbf{S}_h^i(T) = \text{span}\{\boldsymbol{\phi}_{j,T} : 1 \le j \le 7\}$, and the global CR-$P_1$-$P_0$ IFE space is defined to be

$$\mathbf{S}_h(\mathcal{T}_h) = \Big\{ \boldsymbol{v} = (v_1, v_2, v_p)^t \in [L^2(\Omega)]^3 : \boldsymbol{v} \text{ satisfies conditions } \mathbf{C1\text{-}C3} \}. \tag{23}$$

C1: : $\boldsymbol{v}|_T \in \mathbf{S}_h^n(T),\ \forall T \in \mathcal{T}_h^n$, and $\boldsymbol{v}|_T \in \mathbf{S}_h^i(T)\ \forall T \in \mathcal{T}_h^i$.
C2: : $\int_e [\![v_1]\!]\, ds = 0,\ \forall e \in \mathring{\mathcal{E}}_h$.
C3: : v_2 is continuous at every internal point $(x, y) \in \mathring{\mathcal{N}}_h$.

We can construct the P_1-CR-P_0 IFE space in a similar manner. In this case the edge-value conditions (15) are imposed on the second velocity component, and the nodal-value conditions (16) will apply to the first velocity component. The remaining conditions (17)-(21) are the same. Let $\tilde{\mathbf{S}}_h^i(T)$ be the local P_1-CR-P_0 IFE space, then the corresponding global IFE space $\tilde{\mathbf{S}}_h(\mathcal{T}_h)$ is defined as follows

$$\tilde{\mathbf{S}}_h(\mathcal{T}_h) = \Big\{ \boldsymbol{v} = [v_1, v_2, v_p]^t \in [L^2(\Omega)]^3 : \text{ satisfies conditions } \mathbf{C4\text{-}C6} \Big\}. \tag{24}$$

C4: : $\boldsymbol{v}|_T \in \tilde{\mathbf{S}}_h^n(T),\ \forall T \in \mathcal{T}_h^n$, and $\boldsymbol{v}|_T \in \tilde{\mathbf{S}}_h^i(T)\ \forall T \in \mathcal{T}_h^i$.
C5: : v_1 is continuous at every internal point $(x, y) \in \mathring{\mathcal{N}}_h$.
C6: : $\int_e [\![v_2]\!]\, ds = 0,\ \forall e \in \mathring{\mathcal{E}}_h$.

Remark 1. In many cases, the momentum equation (1) of the Stokes system is written as

$$\frac{\partial \mathbf{u}}{\partial t} - \nabla \cdot (2\mu\epsilon(\mathbf{u}) - p\mathbb{I}) = \mathbf{f} \tag{25}$$

where the stress is expressed using the strain tensor $\epsilon(\mathbf{u}) = (\nabla\mathbf{u} + (\nabla\mathbf{u})^t)/2$. In this setup, the stress jump condition (8) should also be changed to

$$[\![(2\mu\epsilon(\mathbf{u}) - p\mathbb{I})\mathbf{n}]\!]_\Gamma = \mathbf{0}. \tag{26}$$

Since the viscosity coefficient $\mu(\mathbf{x})$ is a (piecewise) constant, the incompressibility condition (2) yields

$$2\mu\nabla \cdot \epsilon(\mathbf{u}) = \mu\Delta\mathbf{u}.$$

Hence, these two equations are equivalent in this case. In construction of IFE shape functions, only (19)-(20) need to be replaced by the following two conditions

$$[\![\mu\left(2\partial_x\phi_{1,j}n_1 + (\partial_y\phi_{1,j} + \partial_x\phi_{2,j})n_2\right) - \phi_{p,j}n_1]\!]_{\overline{DE}} = 0, \tag{27}$$

$$[\![\mu\left((\partial_x\phi_{2,j} + \partial_y\phi_{1,j})n_1 + 2\partial_y\phi_{2,j}n_2\right) - \phi_{p,j}n_2]\!]_{\overline{DE}} = 0. \tag{28}$$

The local CR-P_1-P_0 IFE functions, denoted by $\boldsymbol{\phi}^\epsilon_{j,T}$, and local P_1-CR-P_0 IFE functions, denoted by $\tilde{\boldsymbol{\phi}}^\epsilon_{j,T}$ can be constructed accordingly. The corresponding global IFE spaces are denoted by $\mathbf{S}^\epsilon_h(\mathcal{T}_h)$ and $\tilde{\mathbf{S}}^\epsilon_h(\mathcal{T}_h)$.

3. Properties of the mixed conforming-nonconforming IFE spaces.

In this section, we present some basic properties of the mixed conforming-nonconforming IFE spaces.

Theorem 3.1 (Unisolvency). *The CR-P_1-P_0 IFE shape functions $\boldsymbol{\phi}_{j,T}$, $1 \le j \le 7$ can be uniquely determined by the prescribed edge values, the nodal values, and the mean pressure value, regardless of the interface locations and the jumps of viscosity coefficients $\mu^\pm > 0$.*

Proof. We show the unisolvency by considering the invertibility of the coefficient matrices $M_{\rm I}$, $M_{\rm II}$, and $M_{\rm III}$. For the Type I interface triangle, by direct calculation we have

$$\det(M_{\rm I}) = -4\Big(d^4(1-de)+d^2e^2(2-d-e)+e^4(1-d)+\rho de(d^4+de^2+d^2e^2+e^3)\Big) < 0.$$

For the Type II interface element, we have

$$\det(M_{\rm II}) = D_1 + \rho D_2$$

where

$$\begin{aligned}
D_1 &= -4(1-d)e\Big((-1+d)^4 + 4(-1+d)^3e + 7(-1+d)^2e^2 + (-5+6d)e^3 + 2e^4\Big)\\
&= -4(1-d)e\Big((1-d)^3 - 4(1-d)^3e + 7(1-d)^2e^2 - 6(1-d)e^3 + e^3 + 2e^4\Big)\\
&\le -4(1-d)e\Big((1-d)^3 - 4(1-d)^3e + 7(1-d)^2e^2 - 6(1-d)e^3 + 3e^4\Big)\\
&= -4(1-d)e\Big((1-d)^2(1-d-2e)^2 + 3e^2(1-d-e)^2\Big) < 0,
\end{aligned}$$

and with $s = 1-d$, we have

$$\begin{aligned}
D_2 &= -4\Big(4e^2(e-s)^2 + s^2(2e-s)^2\Big) - 4es\Big(2e^4 + e^3(1-6s) + 7e^2s^2 - 4es^3 + s^4\Big)\\
&\le -4\Big(4e^2(e-s)^2 + s^2(2e-s)^2\Big) - 4es\Big(3e^4 - 6e^3s + 7e^2s^2 - 4es^3 + s^4\Big)\\
&= -4\Big(4e^2(e-s)^2 + s^2(2e-s)^2\Big) - 4es\Big(3e^2(e-s)^2 + s^2(2e-s)^2\Big) < 0.
\end{aligned}$$

For the Type III interface element, we have

$$\det(M_{\mathrm{III}}) = D_3 + \rho D_4$$

where

$$\begin{aligned} D_3 &= -4(-1+d)^2\Big(1-2(-1+d)^2d+d(-4+d(-1+2d))e \\ &\quad -(-2+d)(1+2d)e^2+(-2+d)e^3\Big) \\ &= -4s^2\Big(s(1-t)^2t+s^2(1-t)+t(2s^3+t^2-2s^2t)\Big) \\ &\leq -4s^2\Big(s(1-t)^2t+s^2(1-t)+ts^3+t(s^2-t)^2\Big) < 0 \end{aligned}$$

and with $s = 1-d$ and $t = 1-e$,

$$D_4 = -4\Big(3s^4-9s^3t+s^4t-2s^5t+8s^2t^2+2s^3t^2+2s^4t^2-4st^3-s^2t^3-s^3t^3+t^4\Big) < 0.$$

The determinants of coefficient matrices are uniformly nonzero for all $0 \leq d \leq 1$, $0 \leq e \leq 1$, $\rho > 0$ and for all three types of interface elements. This ensures the unisolvency of the IFE functions. □

The following theorems provide basic properties of the new IFE functions. The proofs of these results can be verified by direct calculation, hence we omit the proof in this paper. For more details, we refer the readers to some earlier references [1, 20].

Theorem 3.2 (**Consistency**). *Let $T \in \mathcal{T}_h^i$ be an interface triangle.*

- *If $\mu^+ = \mu^-$, the IFE shape functions $\boldsymbol{\phi}_{j,T}$ become the FE shape functions $\boldsymbol{\psi}_{j,T}$, $1 \leq j \leq 7$.*
- *If the interface moves out of a triangle T, i.e.,*

$$\frac{\min\{|T^-|, |T^+|\}}{|T|} \to 0, \tag{29}$$

the IFE shape functions $\boldsymbol{\phi}_{j,T}$ become the FE shape functions $\boldsymbol{\psi}_{j,T}$, $1 \leq j \leq 7$.

Remark 2. The consistency (29) enables us to use IFE functions for solving Stokes moving interface problem efficiently. In fact, as the interface moves out of an element, the IFE functions smoothly convert to the FE functions. No extra condition is needed to enforce this transition.

Theorem 3.3 (**Continuity of Velocity**). *Let $T \in \mathcal{T}_h^i$ be an interface element and $\boldsymbol{\phi}_{j,T}$ be the vector-valued shape functions. Then the velocity components $\phi_{i,j} \in C(T)$, for $i = 1, 2$, and $j = 1, 2, \cdots, 7$.*

Theorem 3.4 (**Partition of Unity**). *Let $T \in \mathcal{T}_h^i$ be an interface element. The vector-valued IFE shape functions $\boldsymbol{\phi}_{j,T}$, $j = 1, 2, \cdots, 7$, satisfy the partition of unity property, namely: for any $(x, y) \in T$.*

$$\sum_{j=1}^{3} \boldsymbol{\phi}_{j,T}(x,y) = \begin{pmatrix} 1 \\ 0 \\ 0 \end{pmatrix}, \quad \sum_{j=4}^{6} \boldsymbol{\phi}_{j,T}(x,y) = \begin{pmatrix} 0 \\ 1 \\ 0 \end{pmatrix}, \quad \boldsymbol{\phi}_{7,T}(x,y) = \begin{pmatrix} 0 \\ 0 \\ 1 \end{pmatrix}. \tag{30}$$

4. **Semi-discrete and full-discrete schemes.** In this section, we first derive the weak form of the unsteady Stokes interface problem (1)-(8), and then develop the semi-discrete and full-discrete IFE schemes. We use $(\cdot, \cdot)_\omega$ to denote the L^2 inner product on a subset $\omega \subset \Omega$. We will omit the subscript ω if $\omega = \Omega$.

4.1. **Weak formulation.** Taking the inner product with $\mathbf{v} \in [H_0^1(\Omega)]^2$ on the equation (1) and integrating by parts over Ω^- yields,

$$(\mathbf{u}_t, \mathbf{v})_{\Omega^-} + (\mu\nabla\mathbf{u} - p\mathbb{I}, \nabla\mathbf{v})_{\Omega^-} - ((\mu\nabla\mathbf{u} - p\mathbb{I})\mathbf{n}_{\partial\Omega^-}, \mathbf{v})_{\partial\Omega^-} = (\mathbf{f}, \mathbf{v})_{\Omega^-}.$$

Here the second term is the inner product of two tensors $\mathbb{A} = [A_{ij}]$ and $\mathbb{B} = [B_{ij}]$, which is defined by $(\mathbb{A}, \mathbb{B}) := \sum_{i,j}(A_{ij}, B_{ij})$. Note that $\mathbf{n}_\Gamma$ is pointing from Ω^- to Ω^+ and $\mathbf{v}$ vanishes on the outer boundary $\partial\Omega$. We have

$$(\mathbf{u}_t, \mathbf{v})_{\Omega^-} + (\mu\nabla\mathbf{u} - p\mathbb{I}, \nabla\mathbf{v})_{\Omega^-} - ((\mu\nabla\mathbf{u} - p\mathbb{I})\mathbf{n}_\Gamma, \mathbf{v})_\Gamma = (\mathbf{f}, \mathbf{v})_{\Omega^-}.$$

Similar argument applying to the subdomain Ω^+ yields

$$(\mathbf{u}_t, \mathbf{v})_{\Omega^+} + (\mu\nabla\mathbf{u} - p\mathbb{I}, \nabla\mathbf{v})_{\Omega^+} + ((\mu\nabla\mathbf{u} - p\mathbb{I})\mathbf{n}_\Gamma, \mathbf{v})_\Gamma = (\mathbf{f}, \mathbf{v})_{\Omega^+}.$$

Adding the above two equations together, and applying the interface jump condition (8), we have

$$(\mathbf{u}_t, \mathbf{v}) + (\mu\nabla\mathbf{u}, \nabla\mathbf{v}) - (p, \nabla\cdot\mathbf{v}) = (\mathbf{f}, \mathbf{v}).$$

Multiplying $q \in L^2(\Omega)$ to (2), and integrating by parts we have

$$(q, \nabla\cdot\mathbf{u}) = 0. \tag{31}$$

Define the bilinear form and the linear form

$$a(\mathbf{w}, \mathbf{v}) = (\mu\nabla\mathbf{w}, \nabla\mathbf{v}), \qquad \forall\ \mathbf{w}, \mathbf{v} \in [H_0^1(\Omega)]^2, \tag{32}$$

$$b(\mathbf{v}, q) = -(q, \nabla\cdot\mathbf{v}), \qquad \forall\ \mathbf{v} \in [H_0^1(\Omega)]^2,\ \forall\ q \in L_0^2(\Omega). \tag{33}$$

Here, $L_0^2(\Omega) = \{q \in L^2(\Omega) : \int_\Omega q d\mathbf{x} = 0\}$. The weak form of the unsteady Stokes interface problem (1)-(8) is given as follows.

Weak Form: Find $\mathbf{u} \in H^1(0, T; [H_0^1(\Omega)]^2)$ and $p \in L^2(0, T; L_0^2(\Omega))$ such that for each $t \in [0, T]$

$$(\mathbf{u}_t, \mathbf{v}) + a(\mathbf{u}, \mathbf{v}) + b(\mathbf{v}, p) = (\mathbf{f}, \mathbf{v}),\ \forall\ \mathbf{v} \in [H_0^1(\Omega)]^2, \tag{34}$$

$$b(\mathbf{u}, q) = 0,\ \forall\ q \in L_0^2(\Omega), \tag{35}$$

and subject to the initial conditions $\mathbf{u}(\mathbf{x}, 0) = \mathbf{u}_0(\mathbf{x})$, $p(\mathbf{x}, 0) = p_0(\mathbf{x})$.

4.2. **Semi-discrete scheme.** For semi-discretization in space, we use the CR-P_1-P_0 IFE space $\mathbf{S}_h(\mathcal{T}_h)$ to approximate to approximate $[H_0^1(\Omega)]^2 \times L^2(\Omega)$. We write the vector-valued IFE space $\mathbf{S}_h(\mathcal{T}_h) = U_{1h} \times U_{2h} \times W_h$. Then we propose the semi-discrete scheme as follows.

Semi-discrete IFE Scheme: Find $(\mathbf{u}_h, p_h) := (u_{1h}, u_{2h}, p_h) \in H^1(0, T; U_{1h}) \times H^1(0, T; U_{2h}) \times L^2(0, T; W_h)$ such that

$$(\partial_t\mathbf{u}_h, \mathbf{v}_h) + a(\mathbf{u}_h, \mathbf{v}_h) + b(\mathbf{v}_h, p_h) = (\mathbf{f}_h, \mathbf{v}_h),\ \forall\mathbf{v}_h \in U_{1h} \times U_{2h}, \tag{36}$$

$$b(\mathbf{u}_h, q_h) = 0,\ \forall q_h \in W_h, \tag{37}$$

and subject to the initial conditions

$$\mathbf{u}_h(\mathbf{x}, 0) = \mathbf{u}_{0,h}(\mathbf{x}),\ p(\mathbf{x}, 0) = p_{0,h}(\mathbf{x}), \tag{38}$$

where $\mathbf{u}_{0,h}$ and $p_{0,h}$ are some approximations (e.g. the interpolation) of $\mathbf{u}_0$ and p_0 in $U_{1h} \times U_{2h}$ and W_h. We rewrite the semi-discrete scheme in the following matrix form.

Matrix Form: Find the vector function $\mathbf{U}(t)$ such that

$$M(t)\mathbf{U}'(t) + A(t)\mathbf{U}(t) = \mathbf{F}(t), \tag{39}$$

$$\mathbf{U}(0) = \mathbf{U}^0, \tag{40}$$

where $M(t)$ and $A(t)$ denote the IFE mass and stiffness matrices, and $\mathbf{F}(t)$ is the vector corresponding to the right-hand side of (36)-(37). The initial vector $\mathbf{U}^0$ takes the values of the coefficients of the interpolation $\mathbf{I}_h(\mathbf{u}_0, p_0)$. More details will be given in Section 5.

Remark 3. Since the interface $\Gamma(t)$ is a function of time t, the IFE spaces $\mathbf{S}_h(\mathcal{T}_h) = U_{1h} \times U_{2h} \times W_h$ depend on the interface location; hence they are time-dependent. Although the background mesh $\mathcal{T}_h$ is time-independent, the collections of interface elements $\mathcal{T}_h^{i(t)}$ and non-interface elements $\mathcal{T}_h^{n(t)}$ vary by time. That is why the mass matrix $M(t)$ and stiffness matrix $A(t)$ are both time-dependent.

4.3. **Full-discrete scheme.** Let $0 = t_0 < t_1 < \cdots < t_{N-1} < t_N = T$ be a partition of the time interval $[0, T]$ with the uniform step size τ, i.e., $\tau = T/N$, and $t_n = n\tau$. Evaluating (39) at $t = t_{n+\theta} := t_n + \theta\Delta t$, we have

$$M(t_{n+\theta})\mathbf{U}'(t_{n+\theta}) + A(t_{n+\theta})\mathbf{U}(t_{n+\theta}) \quad = \quad \mathbf{F}(t_{n+\theta}). \tag{41}$$

Using the following finite-difference approximations in (41)

$$\begin{aligned} M(t_{n+\theta})\mathbf{U}'(t_{n+\theta}) &\approx M(t_{n+\theta})\frac{\mathbf{U}(t_{n+1}) - \mathbf{U}(t_n)}{\tau} \\ &\approx \frac{1}{\tau}\Big(M(t_{n+1})\mathbf{U}(t_{n+1}) - M(t_n)\mathbf{U}(t_n)\Big), && (42) \\ A(t_{n+\theta})\mathbf{U}(t_{n+\theta}) &\approx (1-\theta)A(t_n)\mathbf{U}(t_n) + \theta A(t_{n+1})\mathbf{U}(t_{n+1}), && (43) \\ \mathbf{F}(t_{n+\theta}) &\approx (1-\theta)\mathbf{F}(t_n) + \theta\mathbf{F}(t_{n+1}), && (44) \end{aligned}$$

we can obtain the following full-discrete IFE scheme.

Full-discrete IFE Scheme: Given initial vector $\mathbf{U}^0$, find $\mathbf{U}^{n+1}$ for each $n = 0, 1, \cdots, N-1$ in

$$\left(\frac{1}{\tau}M^{n+1} + \theta A^{n+1}\right)\mathbf{U}^{n+1} = \left(\frac{1}{\tau}M^n - (1-\theta)A^n\right)\mathbf{U}^n + (1-\theta)\mathbf{F}^n + \theta\mathbf{F}^{n+1}. \tag{45}$$

Note that when $\theta = 1$, the method becomes the **Backward-Euler method**:

$$\left(\frac{1}{\tau}M^{n+1} + A^{n+1}\right)\mathbf{U}^{n+1} = \frac{1}{\tau}M^n\mathbf{U}^n + \mathbf{F}^{n+1}. \tag{46}$$

When $\theta = \frac{1}{2}$, the method is the **Crank-Nicolson method**:

$$\left(\frac{1}{\tau}M^{n+1} + \frac{1}{2}A^{n+1}\right)\mathbf{U}^{n+1} = \left(\frac{1}{\tau}M^n - \frac{1}{2}A^n\right)\mathbf{U}^n + \frac{1}{2}(\mathbf{F}^n + \mathbf{F}^{n+1}). \tag{47}$$

Remark 4. For the time-dependent Stokes interface problem with a stationary interface, i.e. Γ is time-independent, the matrices M and A in the full-discrete scheme (45) will remain unchanged as time evolves. As a result, at each time level, only the vector $\mathbf{F}^n$ needs to be updated.

Remark 5. For the time-dependent Stokes interface problem with a moving interface, although the matrices M^n and A^n depend on the location of interface, which further depends on time, these matrices can be efficiently generated by locally modifying the matrices from the previous time step. A unique feature of IFEM is that not only is the computational mesh interface independent, but the number as well as the location of the unknowns also remain unchanged. In two consecutive time steps, only a small portion of elements change their interface configurations, as shown in Figure 5 marked in dark yellow color. Consequently, we only need to modify local

stiffness and mass matrices on those elements. The majority of the global matrices remain unchanged. This feature is also important in the error analysis of IFE methods for moving interface problems, see [10].

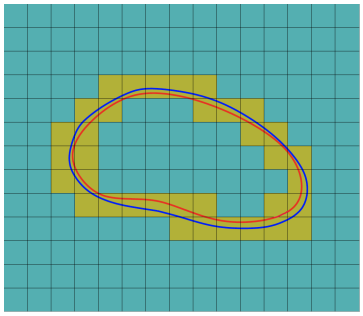

FIGURE 5. An illustration of a moving interface in two consecutive steps. Elements in dark yellow indicate interface configuration changes, and elements in dark blue remain unchanged.

5. **Numerical examples.** In this section, we report some numerical experiments for the mixed conforming-nonconforming IFE methods for the Stokes interface problems. We test both the interpolation and the IFE solution with various configurations of the interface and coefficient jumps. All of our numerical experiments are performed on a family of Cartesian triangular meshes which are obtained by first partitioning the domain into $N_s \times N_s$ congruent rectangles, and then further dividing each rectangle into two triangles by its diagonal with the positive slope.

We investigate the approximation property of IFE space by the interpolation. Define the CR-P_1-P_0 IFE interpolation operator is defined to be $\mathbf{I}_h : H^1(\Omega) \times C(\Omega) \times L^2(\Omega) \to \mathbf{S}_h(\mathcal{T}_h)$ such that

$$\mathbf{I}_h(\mathbf{u},p)|_T = \mathbf{I}_{h,T}(\mathbf{u},p) = \begin{cases} \sum_{j=1}^7 c_j \boldsymbol{\phi}_{j,T}, & \text{if } T \in \mathcal{T}_h^i, \\ \sum_{j=1}^7 c_j \boldsymbol{\psi}_{j,T}, & \text{if } T \in \mathcal{T}_h^n, \end{cases} \tag{48}$$

where $\boldsymbol{\phi}_{j,T}$ and $\boldsymbol{\psi}_{j,T}$ are the local IFE/FE shape functions given in (14) and (11), respectively. For a fixed t, the coefficients c_j take the values

$$c_j = \frac{1}{|e_j|}\int_{e_j} u_1(x,y)ds,\ 1 \le j \le 3, \qquad c_j = u_2(A_{j-3}),\ 4 \le j \le 6,$$

and

$$c_7 = \frac{1}{|T|}\int_T p(x,y)dxdy,$$

where A_j and e_j, $j = 1,2,3$ are the vertices and edges of the the triangle T, respectively. The P_1-CR-P_0 interpolation can be defined similarly. The errors of the IFE interpolations are measured in L^2 and semi-H^1 norms as follows

$$e^0(u_{1,I}) = \|u_1 - u_{1,I}\|_{L^2(\Omega)},\ e^0(u_{2,I}) = \|u_2 - u_{2,I}\|_{L^2(\Omega)},\ e^0(p_I) = \|p - p_I\|_{L^2(\Omega)},$$
$$e^1(u_{1,I}) = |u_1 - u_{1,I}|_{H^1(\Omega)},\ e^1(u_{2,I}) = |u_2 - u_{2,I}|_{H^1(\Omega)},$$

where $u_{1,I}$, $u_{2,I}$, p_I are components of the vector-valued function $\mathbf{I}_h(\mathbf{u},p)$. In the tables below, we report the convergence rate based on two consecutive meshes $\mathcal{T}_h$

and $\mathcal{T}_{h/2}$, as well as the overall convergence rate among all meshes using the linear regression.

Example 5.1 (**Interpolation Accuracy**). In this example, we test the approximation capability of the new vector valued IFE space using interpolation. Since the interpolation is a time-independent procedure, we use a steady-state solution given in [1, 20] for this experiment. Let the domain be $\Omega = [-1, 1]^2$ and the interface be $\Gamma = \{(x, y) : x^2 + y^2 = 0.3\}$. The circular interface separates the domain Ω into two subdomains $\Omega^- = \{(x, y) : x^2 + y^2 < 0.3\}$ and $\Omega^+ = \{(x, y) : x^2 + y^2 > 0.3\}$. The exact solutions u_1, u_2 and p are defined as follows:

$$\mathbf{u}(x,y) = \begin{cases} u_1 = \begin{cases} \frac{y(x^2+y^2-0.3)}{\mu^+}, & \text{if } (x,y) \in \Omega^+, \\ \frac{y(x^2+y^2-0.3)}{\mu^-}, & \text{if } (x,y) \in \Omega^-, \end{cases} \\ u_2 = \begin{cases} \frac{-x(x^2+y^2-0.3)}{\mu^+}, & \text{if } (x,y) \in \Omega^+, \\ \frac{-x(x^2+y^2-0.3)}{\mu^-}, & \text{if } (x,y) \in \Omega^-, \end{cases} \end{cases} \quad \text{and } p(x,y) = \frac{1}{10}(x^3 - y^3). \tag{49}$$

We first test a moderate coefficient contrast with $\mu^- = 1$ and $\mu^+ = 10$. Tables 1-2 report the interpolation errors using CR-P_1-P_0 and P_1-CR-P_0 IFE functions, respectively. We can see from these tables that the accuracy of these two IFE spaces are similar. Both of these interpolation errors obey

$$e^0(u_{i,I}) \approx \mathcal{O}(h^2), \ e^1(u_{i,I}) \approx \mathcal{O}(h), \ e^0(p_I) \approx \mathcal{O}(h), \tag{50}$$

where $i = 1, 2$.

TABLE 1. CR-P_1-P_0 IFE Interpolation errors for Example 5.1 with $\mu^- = 1$ and $\mu^+ = 10$.

N	$e^0(u_{1,I})$	rate	$e^0(u_{2,I})$	rate	$e^0(p_I)$	rate	$e^1(u_{1,I})$	rate	$e^1(u_{2,I})$	rate
8	5.36e-3	n/a	1.15e-2	n/a	7.02e-2	n/a	1.21e-1	n/a	1.54e-1	n/a
16	1.39e-3	1.95	3.03e-3	1.92	3.14e-2	1.16	5.80e-2	1.06	7.32e-2	1.06
32	3.59e-4	1.95	7.84e-4	1.95	1.46e-2	1.10	2.85e-2	1.02	3.73e-2	0.96
64	9.20e-5	1.96	2.03e-4	1.95	5.28e-3	1.47	1.45e-2	0.98	1.91e-2	0.97
128	2.33e-5	1.98	5.14e-5	1.98	2.10e-3	1.33	7.34e-3	0.98	9.66e-3	0.98
256	5.85e-6	1.99	1.29e-5	1.99	8.47e-4	1.31	3.68e-3	1.00	4.85e-3	0.99
rate		1.98		1.96		1.29		1.00		0.99

Next, we test a larger coefficient jump ($\mu^- = 1$ and $\mu^+ = 200$) and a flipped coefficients case ($\mu^- = 10$ and $\mu^+ = 1$). We only report the P_1-CR-P_0 IFE interpolation, since the CR-P_1-P_0 IFE results are close. Errors for large jump and flipped jump cases are listed in Tables 3 - 4, respectively. The convergence rates are again consistent with (50).

Example 5.2 (**Unsteady Stokes Equation with Fixed Interface**). In this example, we consider a time-dependent Stokes equation with a fixed interface. The domain Ω and interface Γ is the same as in Example 5.1. The time domain is set to be $[0, 1]$, and it is partitioned uniformly to N_t subintervals. We use both backward-Euler and Crank-Nicolson schemes with the time step size $\tau = 2h$. The errors are measured at the final time $t = 1$. The initial data $\mathbf{u}_0$, p_0, the boundary condition,

TABLE 2. P_1-CR-P_0 IFE Interpolation errors for Example 5.1 with $\mu^- = 1$ and $\mu^+ = 10$.

N	$e^0(u_{1,I})$	rate	$e^0(u_{2,I})$	rate	$e^0(p_I)$	rate	$e^1(u_{1,I})$	rate	$e^1(u_{2,I})$	rate
8	1.16e-2	n/a	5.44e-3	n/a	1.44e-1	n/a	1.49e-1	n/a	1.30e-1	n/a
16	3.08e-3	1.92	1.42e-3	1.94	5.93e-2	1.29	7.47e-2	1.00	5.80e-2	1.16
32	5.15e-4	1.95	2.36e-4	1.96	2.14e-2	1.18	3.08e-2	0.96	2.37e-2	0.98
64	7.94e-4	1.96	3.65e-4	1.97	2.70e-2	1.14	3.76e-2	0.99	2.88e-2	1.00
128	5.15e-5	1.99	2.34e-5	1.99	3.56e-3	1.43	9.69e-3	0.98	7.35e-3	0.99
256	1.29e-5	1.99	5.86e-6	2.00	1.32e-3	1.43	4.86e-3	0.99	3.68e-3	1.00
rate		1.89		1.90		1.31		0.95		0.98

TABLE 3. P_1-CR-P_0 IFE Interpolation errors for Example 5.1 with $\mu^- = 1$ and $\mu^+ = 200$.

N	$e^0(u_{1,I})$	rate	$e^0(u_{2,I})$	rate	$e^0(p_I)$	rate	$e^1(u_{1,I})$	rate	$e^1(u_{2,I})$	rate
8	1.01e-2	n/a	4.86e-2	n/a	2.81e-0	n/a	1.35e-1	n/a	1.26e-1	n/a
16	2.73e-3	1.88	1.28e-3	1.92	1.21e-0	1.21	6.77e-2	1.00	5.31e-2	1.24
32	7.19e-4	1.93	3.33e-4	1.95	5.75e-1	1.08	3.43e-2	0.98	2.66e-2	1.00
64	1.86e-4	1.95	8.59e-5	1.97	1.98e-2	1.54	1.75e-2	0.97	1.34e-2	0.99
128	4.73e-5	1.98	2.15e-5	1.98	7.26e-2	1.45	8.91e-3	0.98	6.79e-3	0.98
256	1.19e-5	1.99	5.40e-6	1.99	2.59e-2	1.49	4.49e-3	0.99	3.41e-3	0.99
rate		1.95		1.90		1.45		0.98		1.03

TABLE 4. P_1-CR-P_0 IFE Interpolation errors for Example 5.1 with $\mu^- = 10$ and $\mu^+ = 1$.

N_s	$e^0(u_{1,I})$	rate	$e^0(u_{2,I})$	rate	$e^0(p_I)$	rate	$e^1(u_{1,I})$	rate	$e^1(u_{2,I})$	rate
8	5.11e-2	n/a	2.32e-2	n/a	3.38e-1	n/a	6.04e-1	n/a	4.61e-1	n/a
16	1.29e-2	1.99	5.82e-3	1.99	9.59e-2	1.82	3.02e-1	1.00	2.29e-1	1.01
32	3.23e-3	1.99	1.46e-3	2.00	2.36e-2	2.03	1.51e-1	1.00	1.15e-1	1.00
64	8.09e-4	2.00	3.66e-4	2.00	1.07e-2	1.14	7.58e-2	1.00	5.73e-2	1.00
128	2.02e-4	2.00	9.14e-5	2.00	3.41e-3	1.65	3.79e-2	1.00	2.87e-2	1.00
256	5.06e-5	2.00	2.29e-5	2.00	1.37e-3	1.32	1.90e-2	1.00	1.43e-2	1.00
rate		2.00		2.00		1.58		1.00		1.00

and the source term $\mathbf{f}$ are chosen so that the exact solutions of this problem are as follows

$$\mathbf{u}(x,y,t) = \begin{cases} u_1 = \begin{cases} \frac{y(x^2+y^2-0.3)}{\mu^+} e^{3t}, & \text{if } (x,y) \in \Omega^+, \\ \frac{y(x^2+y^2-0.3)}{\mu^-} e^{3t}, & \text{if } (x,y) \in \Omega^-, \end{cases} \\ u_2 = \begin{cases} \frac{-x(x^2+y^2-0.3)}{\mu^+} e^{3t}, & \text{if } (x,y) \in \Omega^+, \\ \frac{-x(x^2+y^2-0.3)}{\mu^-} e^{3t}, & \text{if } (x,y) \in \Omega^-, \end{cases} \end{cases} \qquad p(x,y) = \frac{1}{10}(x^3 - y^3). \tag{51}$$

Table 5 and Table 6 report the backward-Euler and the Crank-Nicolson IFE solutions at the final time $t = 1$, respectively. The numerical results indicate that the errors of Crank-Nicolson are a little smaller than those of backward-Euler. They

obey the expected convergence rates

$$e^0(u_{ih}) \approx \mathcal{O}(h^2+\tau^k),\ e^1(u_{ih}) \approx \mathcal{O}(h+\tau^k),\ e^0(p_h) \approx \mathcal{O}(h+\tau^k), \tag{52}$$

where $i = 1, 2$, and $k = 1$ for backward-Euler, and $k = 2$ for Crank-Nicolson. As before, we report only the P_1-CR-P_0 IFE solutions, and the results for the CR-P_1-P_0 IFE solution are similar.

TABLE 5. P_1-CR-P_0 backward-Euler IFE solutions for Example 5.2 at $t = 1$ with $\mu^- = 1$ and $\mu^+ = 10$.

N	$e^0(u_{1,I})$	rate	$e^0(u_{2,I})$	rate	$e^0(p_I)$	rate	$e^1(u_{1,I})$	rate	$e^1(u_{2,I})$	rate
8	2.49e-1	n/a	1.72e-1	n/a	9.46e-0	n/a	2.95e-0	n/a	2.83e-0	n/a
16	6.86e-2	1.86	4.70e-2	1.87	4.70e-0	1.01	1.51e-0	0.97	1.38e-0	1.03
32	1.69e-2	2.02	1.18e-2	1.99	2.44e-0	0.95	7.65e-1	0.98	7.14e-1	0.96
64	3.87e-3	2.13	3.54e-3	1.74	1.15e-0	1.08	3.94e-1	0.96	3.69e-1	0.95
128	1.57e-3	1.31	1.65e-3	1.10	6.23e-1	0.88	2.04e-1	0.95	1.91e-1	0.95
256	8.69e-4	0.85	9.07e-4	0.86	3.35e-1	0.90	1.07e-1	0.93	1.02e-1	0.91
rate		1.69		1.54		0.97		0.96		0.96

TABLE 6. P_1-CR-P_0 Crank-Nicolson IFE solutions for Example 5.2 at $t = 1$ with $\mu^- = 1$ and $\mu^+ = 10$.

N	$e^0(u_{1,I})$	rate	$e^0(u_{2,I})$	rate	$e^0(p_I)$	rate	$e^1(u_{1,I})$	rate	$e^1(u_{2,I})$	rate
8	2.51e-1	n/a	1.72e-1	n/a	9.02e-0	n/a	2.94e-0	n/a	2.79e-0	n/a
16	7.25e-2	1.79	5.02e-2	1.77	4.51e-0	1.00	1.50e-0	0.97	1.36e-0	1.04
32	1.92e-2	1.92	1.39e-2	1.85	2.34e-0	0.94	7.62e-1	0.98	6.98e-1	0.96
64	4.33e-3	2.15	3.27e-3	2.09	1.11e-0	1.08	3.92e-1	0.96	3.61e-1	0.95
128	9.96e-4	2.12	7.94e-4	2.04	5.97e-1	0.89	2.03e-1	0.95	1.87e-1	0.95
256	2.39e-4	2.06	2.33e-4	1.76	3.20e-1	0.90	1.06e-1	0.93	1.02e-1	0.91
rate		2.03		1.93		0.97		0.96		0.96

Example 5.3 (Unsteady Stokes Equation: Circular Moving Interface). In this example we test our mixed IFE method on a Stokes moving interface problem. The interface curve is a circle centered at origin with a varying radius. The function for the interface curve is given as

$$\Gamma(x, y, t) = x^2 + y^2 - 0.3\left(\frac{1}{2}\sin(2\pi t) + 1\right).$$

It can be seen that at time $t = 0$, the interface is the same as Example 5.2 with a radius of $r = 0.54772$. As the time t increases, the radius will first increase, then decrease, and finally return to the original one. The maximum and minimum radius $r_{max} = 0.67082$ and $r_{min} = 0.3873$ occur at $t = 0.25$ and $t = 0.75$, as shown in Figure 6. The exact solution $\mathbf{u}$ is written in terms of the level-set interface function

$\Gamma = 0$:

$$\mathbf{u}(x,y,t) = \begin{cases} u_1 = \begin{cases} \frac{1}{\mu^+} y\Gamma(x,y,t), & \text{if } (x,y) \in \Omega^+(t), \\ \frac{1}{\mu^-} y\Gamma(x,y,t), & \text{if } (x,y) \in \Omega^-(t), \end{cases} \\ u_2 = \begin{cases} -\frac{1}{\mu^+} x\Gamma(x,y,t), & \text{if } (x,y) \in \Omega^+(t), \\ -\frac{1}{\mu^-} x\Gamma(x,y,t), & \text{if } (x,y) \in \Omega^-(t), \end{cases} \end{cases} \qquad p(x,y) = \frac{1}{10}(x^3 - y^3). \tag{53}$$

In this experiment, we set the time step size $\tau = h$. We first test the moderate jump case for this moving interface problem. Table 7 reports the errors at the final time level of the backward-Euler IFE solutions. The error decay is observed to converge in an optimal order, as stated in (52). Figure 6 shows the IFE solution u_1 and u_2 at time $t = 0.25$, $t = 0.75$, and $t = 1$, respectively, on the 64×64 mesh. For a larger jump case, the errors are reported in Table 8.

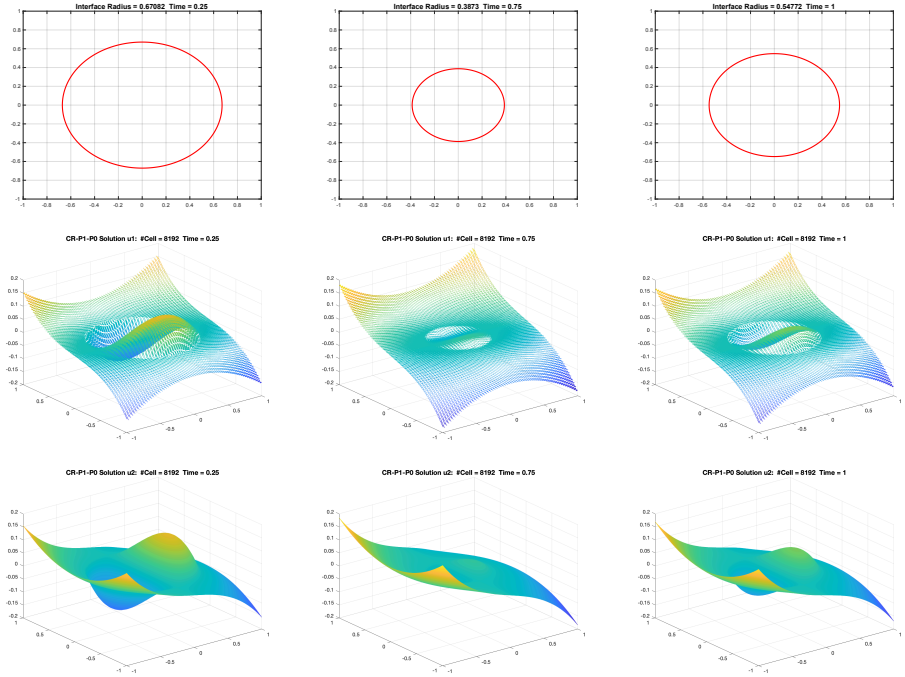

FIGURE 6. CR-P_1-P_0 IFE Solution of Example 5.3 with $\mu^- = 1$ and $\mu^+ = 10$ on the 64×64 mesh at times $t = 0.25$, 0.75, and 1. Top plots: Interfaces, middle: IFE solutions u_{1h}, bottom: IFE solutions u_{2h}.

The condition numbers of the IFE systems are reported in Tables 9 and 10. We monitor the condition numbers at $t = 0.25$, $t = 0.75$, and $t = 1$ which correspond to the interface circle listed in Figure 6. We test different contrast ratios by fixing the coefficient $\mu^- = 1$ and varying the other coefficient $\mu^+ = 0.01$, 0.1, 1, 10, and 100. Note that when $\mu^+ = 1$, there is no jump in coefficient, hence the IFE scheme becomes the standard FE scheme. Even in this no-jump case, we observe that the

TABLE 7. CR-P_1-P_0 Backward-Euler IFE solution for Example 5.3 at $t = 1$ with $\mu^- = 1$ and $\mu^+ = 10$.

N	$e^0(u_{1,I})$	rate	$e^0(u_{2,I})$	rate	$e^0(p_I)$	rate	$e^1(u_{1,I})$	rate	$e^1(u_{2,I})$	rate
8	7.85e-3	n/a	1.14e-2	n/a	4.83e-1	n/a	1.36e-1	n/a	1.51e-1	n/a
16	2.05e-3	1.94	2.95e-3	1.95	2.41e-1	1.00	7.02e-2	0.95	7.45e-2	1.02
32	5.13e-4	2.00	6.54e-4	2.17	1.24e-1	0.96	3.57e-2	0.98	3.82e-2	0.96
64	1.68e-4	1.61	1.32e-4	2.30	5.78e-2	1.10	1.84e-2	0.96	1.96e-2	0.96
128	8.54e-5	0.98	6.68e-5	0.99	3.12e-2	0.89	9.52e-3	0.95	1.01e-2	0.95
rate		1.67		1.93		1.00		0.96		0.97

TABLE 8. CR-P_1-P_0 Backward-Euler IFE solution for Example 5.3 at $t = 1$ with $\mu^- = 1$ and $\mu^+ = 200$.

N	$e^0(u_{1,I})$	rate	$e^0(u_{2,I})$	rate	$e^0(p_I)$	rate	$e^1(u_{1,I})$	rate	$e^1(u_{2,I})$	rate
8	1.17e-2	n/a	1.29e-2	n/a	1.25e-0	n/a	1.44e-1	n/a	1.41e-1	n/a
16	3.86e-3	1.60	4.56e-3	1.50	8.16e-1	0.61	7.99e-2	0.85	7.01e-1	1.01
32	1.20e-3	1.69	1.42e-3	1.69	5.10e-1	0.68	3.80e-2	1.07	3.56e-2	0.98
64	2.02e-4	2.57	2.50e-4	2.50	2.00e-1	1.35	1.74e-2	1.12	1.78e-2	1.00
128	3.48e-5	2.54	4.21e-5	2.57	8.70e-2	1.20	8.43e-3	1.05	9.01e-3	0.98
rate		2.10		2.07		0.97		1.04		1.04

condition number is of order $\mathcal{O}(h^{-4})$. We also observe that the condition number increases as the jump ratio enlarges. No significant differences have been noticed for backward-Euler and Crank-Nicolson in terms of the conditions numbers.

TABLE 9. Condition Number for Backward-Euler CR-P_1-P_0 Example 5.3 with $\mu^- = 1$.

	N_s	$\mu^+ = 0.01$	$\mu^+ = 0.1$	$\mu^+ = 1$	$\mu^+ = 10$	$\mu^+ = 100$
t=0.25	8	3.03e+05	5.94e+04	2.80e+05	1.38e+07	1.31e+09
	16	1.04e+06	7.82e+05	4.36e+06	1.11e+08	1.40e+10
	32	2.69e+08	6.06e+06	6.87e+07	9.06e+08	4.64e+11
	64	6.51e+10	7.07e+07	1.09e+09	8.46e+09	8.48e+12
	128	1.30e+12	7.27e+08	1.74e+10	8.15e+10	6.26e+14
t=0.75	8	2.07e+04	4.24e+04	2.80e+05	1.22e+07	1.78e+09
	16	1.04e+06	7.82e+05	4.36e+06	1.64e+08	2.22e+10
	32	1.15e+08	9.36e+06	6.87e+07	1.67e+09	1.79e+11
	64	2.44e+09	1.11e+08	1.09e+09	1.62e+10	7.07e+13
	128	1.22e+10	9.29e+08	1.74e+10	1.16e+11	2.66e+15
t=1	8	2.34e+06	3.68e+04	2.80e+05	1.26e+07	1.10e+09
	16	7.76e+06	5.65e+05	4.36e+06	1.08e+08	1.94e+10
	32	4.30e+07	8.53e+06	6.87e+07	1.41e+09	1.59e+13
	64	2.99e+08	9.10e+07	1.09e+09	1.05e+10	3.93e+13
	128	7.30e+11	8.24e+08	1.74e+10	9.94e+10	2.72e+15

TABLE 10. Condition Number for Crank-Nicolson CR-P_1-P_0 Example 5.3 with $\mu^- = 1$.

	N_s	$\mu^+ = 0.01$	$\mu^+ = 0.1$	$\mu^+ = 1$	$\mu^+ = 10$	$\mu^+ = 100$
t=0.25	8	4.92e+05	7.56e+04	2.88e+05	1.39e+07	1.32e+09
	16	1.43e+06	9.20e+05	4.42e+06	1.12e+08	1.40e+10
	32	3.29e+08	6.58e+06	6.92e+07	9.08e+08	4.65e+11
	64	7.54e+10	7.37e+07	1.10e+09	8.48e+09	8.48e+12
	128	1.43e+12	7.42e+08	1.74e+10	8.16e+10	6.26e+14
t=0.75	8	3.52e+04	5.61e+04	2.88e+05	1.22e+07	1.78e+09
	16	7.29e+05	8.50e+05	4.42e+06	1.64e+08	2.22e+10
	32	1.51e+08	1.04e+07	6.92e+07	1.67e+09	1.79e+11
	64	3.00e+09	1.17e+08	1.10e+09	1.62e+10	7.08e+13
	128	1.39e+10	9.50e+08	1.74e+10	1.16e+11	2.66e+15
t=1	8	3.29e+06	4.49e+04	2.88e+05	1.26e+07	1.10e+09
	16	1.02e+07	6.54e+05	4.42e+06	1.08e+08	1.95e+10
	32	5.58e+07	9.37e+06	6.92e+07	1.41e+09	1.59e+13
	64	3.71e+08	9.56e+07	1.10e+09	1.06e+10	3.93e+13
	128	8.04e+11	8.42e+08	1.74e+10	9.95e+10	2.73e+15

6. **Conclusion.** In this paper, we developed a mixed conforming-nonconforming immersed finite element method for unsteady Stokes interface problems. The proposed vector-valued IFE spaces use conforming P_1 approximation for one velocity component and nonconforming P_1 approximation for the other. The pressure is approximated by piecewise constant. Unisolvency of the vector-valued IFE functions is proved. Interpolation errors are observed to be optimal which indicates these new IFE spaces have sufficient approximation capabilities. This new IFE function space can be used to solve steady-state, and unsteady Stokes interface problems. In addition, we have extended the application to a moving interface problem, and our numerical results show the optimal convergence in some benchmark tests. The proposed IFE method can be extended to some more general fluid flow interface problems such as Navier-Stokes equations, which will be an interesting future topic to explore.

REFERENCES

[1] S. Adjerid, N. Chaabane and T. Lin, An immersed discontinuous finite element method for Stokes interface problems, *Comput. Methods Appl. Mech. Engrg.*, **293** (2015), 170–190.

[2] D. N. Arnold, On nonconforming linear-constant elements for some variants of the Stokes equations, *Istit. Lombardo Accad. Sci. Lett. Rend. A*, **127** (1993), 83–93.

[3] N. Chaabane, *Immersed and Discontinuous Finite Element Methods*, Thesis (Ph.D.)-Virginia Polytechnic Institute and State University. 2015.

[4] Z. Chen, *Finite Element Methods and their Applications*, Scientific Computation. Springer-Verlag, Berlin, 2005.

[5] Y. Chen and X. Zhang, A P_2-P_1 partially penalized immersed finite element method for Stokes interface problems, *Int. J. Numer. Anal. Model.*, **18** (2021), 120–141.

[6] M. Crouzeix and P.-A. Raviart, Conforming and nonconforming finite element methods for solving the stationary Stokes equations. I, *Rev. Française Automat. Informat. Recherche Opérationnelle Sér. Rouge*, **7** (1973), 33–75.

[7] F. Duarte, R. Gormaz and S. Natesan, Arbitrary Lagrangian-Eulerian method for Navier-Stokes equations with moving boundaries, *Comput. Methods Appl. Mech. Engrg.*, **193** (2004), 4819–4836.

[8] V. Girault and P.-A. Raviart, *Finite Element Methods for Navier-Stokes Equations*, volume 5 of *Springer Series in Computational Mathematics*, Springer-Verlag, Berlin, 1986. Theory and algorithms.
[9] S. Großand A. Reusken, An extended pressure finite element space for two-phase incompressible flows with surface tension, *J. Comput. Phys.*, **224** (2007), 40–58.
[10] R. Guo, Solving parabolic moving interface problems with dynamical immersed spaces on unfitted meshes: Fully discrete analysis, *SIAM J. Numer. Anal.*, **59** (2021), 797–828.
[11] R. Guo and T. Lin, A group of immersed finite element spaces for elliptic interface problems, *IMA J. Numer. Anal.*, **39** (2019), 482–511.
[12] R. Guo, T. Lin and Y. Lin, A fixed mesh method with immersed finite elements for solving interface inverse problems, *J. Sci. Comput.*, **79** (2019), 148–175.
[13] R. Guo, T. Lin and Y. Lin, Recovering elastic inclusions by shape optimization methods with immersed finite elements, *J. Comput. Phys.*, **404** (2020), 109123, 24 pp.
[14] R. Guo, T. Lin and Q. Zhuang, Improved error estimation for the partially penalized immersed finite element methods for elliptic interface problems, *Int. J. Numer. Anal. Model.*, **16** (2019), 575–589.
[15] P. Hansbo, M. G. Larson and S. Zahedi, A cut finite element method for a Stokes interface problem, *Appl. Numer. Math.*, **85** (2014), 90–114.
[16] X. He, T. Lin and Y. Lin, Immersed finite element methods for elliptic interface problems with non-homogeneous jump conditions, *Int. J. Numer. Anal. Model.*, **8** (2011), 284–301.
[17] X. He, T. Lin, Y. Lin and X. Zhang, Immersed finite element methods for parabolic equations with moving interface, *Numer. Methods Partial Differential Equations*, **29** (2013), 619–646.
[18] C. He and X. Zhang, Residual-based a posteriori error estimation for immersed finite element methods, *J. Sci. Comput.*, **81** (2019), 2051–2079.
[19] V. John, *Finite Element Methods for Incompressible Flow Problems*, volume 51 of *Springer Series in Computational Mathematics*, Springer, Cham, 2016.
[20] D. Jones and X. Zhang, A class of nonconforming immersed finite element methods for Stokes interface problems, *J. Comput. Appl. Math.*, **392** (2021), 113493.
[21] R. Kouhia and R. Stenberg, A linear nonconforming finite element method for nearly incompressible elasticity and Stokes flow, *Comput. Methods Appl. Mech. Engrg.*, **124** (1995), 195–212.
[22] R. Lan and P. Sun, A monolithic arbitrary Lagrangian-Eulerian finite element analysis for a Stokes/parabolic moving interface problem, *J. Sci. Comput.*, **82** (2020), Paper No. 59, 36 pp.
[23] J. Li and Z. Chen, A new local stabilized nonconforming finite element method for the Stokes equations, *Computing*, **82** (2008), 157–170.
[24] Z. Li, T. Lin and X. Wu, New Cartesian grid methods for interface problems using the finite element formulation, *Numer. Math.*, **96** (2003), 61–98.
[25] T. Lin, Y. Lin and X. Zhang, A method of lines based on immersed finite elements for parabolic moving interface problems, *Adv. Appl. Math. Mech.*, **5** (2013), 548–568.
[26] T. Lin, Y. Lin and X. Zhang, Partially penalized immersed finite element methods for elliptic interface problems, *SIAM J. Numer. Anal.*, **53** (2015), 1121–1144.
[27] T. Lin, D. Sheen and X. Zhang, A locking-free immersed finite element method for planar elasticity interface problems, *J. Comput. Phys.*, **247** (2013), 228–247.
[28] T. Lin, D. Sheen and X. Zhang, A nonconforming immersed finite element method for elliptic interface problems, *J. Sci. Comput.*, **79** (2019), 442–463.
[29] T. Lin and X. Zhang, Linear and bilinear immersed finite elements for planar elasticity interface problems, *J. Comput. Appl. Math.*, **236** (2012), 4681–4699.
[30] T. Lin and Q. Zhuang, Optimal error bounds for partially penalized immersed finite element methods for parabolic interface problems, *J. Comput. Appl. Math.*, **366** (2020), 112401, 11 pp.
[31] A. Lundberg, P. Sun and C. Wang, Distributed Lagrange multiplier-fictitious domain finite element method for Stokes interface problems, *Int. J. Numer. Anal. Model.*, **16** (2019), 939–963.
[32] R. Rannacher and S. Turek, Simple nonconforming quadrilateral Stokes element, *Numer. Methods Partial Differential Equations*, **8** (1992), 97–111.
[33] B. Rivière, *Discontinuous Galerkin Methods for Solving Elliptic and Parabolic Equations*, volume 35 of *Frontiers in Applied Mathematics*, Society for Industrial and Applied Mathematics (SIAM), Philadelphia, PA, 2008. Theory and implementation.

[34] P. Sun, Fictitious domain finite element method for Stokes/elliptic interface problems with jump coefficients, *J. Comput. Appl. Math.*, **356** (2019), 81–97.
[35] C. Taylor and P. Hood, A numerical solution of the Navier-Stokes equations using the finite element technique, *Internat. J. Comput. & Fluids*, **1** (1973), 73–100.
[36] N. Wang and J. Chen, A nonconforming Nitsche's extended finite element method for Stokes interface problems, *J. Sci. Comput.*, **81** (2019), 342–374.
[37] N. K. Yamaleev, D. C. Del Rey Fernández, J. Lou and M. H. Carpenter, Entropy stable spectral collocation schemes for the 3-D Navier-Stokes equations on dynamic unstructured grids, *J. Comput. Phys.*, **399** (2019), 108897, 27 pp.
[38] M. Zhang and S. Zhang, A 3D conforming-nonconforming mixed finite element for solving symmetric stress Stokes equations, *Int. J. Numer. Anal. Model.*, **14** (2017), 730–743.

Received November 2020; revised February 2021.

E-mail address: dtj70@msstate.edu
E-mail address: xzhang@okstate.edu